Communications in Physics, Vol. 24, No. 3S2 (2014), pp. 71-84
DOI:10.15625/0868-3166/24/3S2/5052

NUMERICAL INVESTIGATIONS OF LASER DIODE END-PUMPED SOLID-STATE Cr^{3+}:LiSAF LASERS PASSIVELY Q-SWITCHED WITH Cr^{4+}:YSO CRYSTAL

NGUYEN VAN HAO
Center for Quantum Electronics, Institute of Physics, Vietnamese Academy of Science and Technology
and
Thai Nguyen University of Science, Thai Nguyen city, Vietnam
PHAM HONG MINH, PHAM VAN DUONG, AND NGUYEN DAI HUNG
Center for Quantum Electronics, Institute of Physics, Vietnamese Academy of Science and Technology
NGUYEN THE BINH
University of Science, Vietnam National University, Hanoi, Vietnam
E-mail: nvhao@grad.iop.vast.ac.vn

Received 04 April 2014
Accepted for publication 24 May 2014

Abstract. *We have numerically investigated, for the first time, the optical performance and characteristics of diode-end-pumped passively Cr^{4+}:YSO Q-switched solid-state Cr^{3+}:LiSAF lasers using a rate equation system extended to multi-wavelength. Homogeneously broadened emission spectra of the laser crystal and broad absorption spectra of Cr^{4+}:YSO saturable absorber have been respected in the investigation. A tunable passively Q-switched laser operation is also developed with a birefringent filter plate used as an intracavity selective element. As a result, improved understanding of passively Q-switched Cr^{4+}:YSO solid-state Cr^{3+}:LiSAF lasers has been obtained in broadband and tunable laser operations. Characteristics of the tunable passively Q-switched Cr^{3+}:LiSAF laser were demonstrated to be clearly dependent on wavelength. The spectro-temporal evolution of a single pulse emitted from the passively Q-switched Cr^{3+}:LiSAF laser has been reported.*

Keywords: Cr:LiSAF, Cr:YSO, saturable absorption, passively Q-switching, solid state laser.

I. INTRODUCTION

Many applications such as LIDAR, remote sensing, nonlinear frequency conversion and material processing require high-energy laser pulses with pulse width in the nanosecond range [1]. For obtain such short laser pulses of high peak power, Q- switching techniques can be used. In Q-switched laser operation, resonator losses can be switched by using active or passive modulation schemes [2]. Compared to active Q-switching, passive Q-switching has been more widely used to develop lower-cost and compact Q-switched lasers. In passively Q-switched lasers, the resonator losses are modulated with saturable absorber, semiconductor saturable absorber mirror (SESAM) [2–12]. Many durable solid-state saturable absorbers have been reported to work effectively for the solid-state laser at various wavelengths. The Cr^{4+}:Y_2SiO_5 (Cr:YSO) has been shown to be an effective saturable absorber to Q switch the ruby laser, the alexandrite laser, and the Cr^{3+}:$LiCaAlF_6$ (Cr:LiCAF) laser [10–12]. Some of the important material properties and parameters of Cr:YSO are shown in Table 1.

The Cr:LiSAF solid-state laser, discovered by Payne *et al.* at firstly in 1989 [14], has a broad gain band from 780 nm to 920 nm. The Cr:LiSAF has been paid great attention in the tunable and shortly pulsed laser technology [3–13, 15–18]. The Cr:LiSAF has a long fluorescence lifetime (67 μs) and an effective Q-switched operation with the peak wavelength of the free-running laser spectrum is near 850 nm [2, 16, 19]. The Cr:LiSAF exhibits a broad emission spectrum, long lifetime of the upper laser level, low nonlinear refractive index, and low excited-state absorption that make it a unique source for tunable or short pulse lasers. The LiSAF host crystal is uniaxial and the Cr^{3+} emission is strongly π-polarized (E//c). The peak of the ${}^4T_2 \rightarrow {}^4A_2$ emission spectrum occurs at 830 nm and has a cross-section of 4.8×10^{-20} cm^2. It has been assumed that Cr^{3+} ions in LiSAF crystal have a homogeneously broadened emission line for the ${}^4T_2 \rightarrow {}^4A_2$ transition [14]. Owing to the internal absorption caused by ${}^4A_2 \rightarrow {}^4T_2$ transitions, the laser emission spectrum is red-shifted to be peaked near 850 nm. Some of the important material properties of Cr:LiSAF parameters are shown in Table 2.

The laser performances of passively Q-switched Cr:LiSAF and Cr:LiCAF lasers were studied experimentally and numerically [3–6, 10–19], however, these works were only done at the single frequency analysis and almost of the laser systems were flash lamp-pumped. As shown in Table 1 and Table 2, emission spectra of Cr:LiSAF crystal and absorption spectra of Cr:YSO are broadband. In practice, experimentally measured and computed bandwidths of the passively Q-switched Cr:LiSAF (and Cr:LiCAF) laser emissions were quite broad as high as 10 nm [3-6, 13, 14]. Consequently, such a single- frequency analysis is impossible to understand better the spectro-temporal evolution and wavelength-dependent characteristics... of the passively Q-switched laser operations. Furthermore, CW laser diode end-pumping has been widely used to develop passively Q-switched Cr:LiSAF and Cr:LiCAF laser systems.

In this paper, we have numerically investigated, for the first time, the optical performance and characteristics of CW diode-end-pumped and passively Cr^{4+}:YSO Q-switched Cr^{3+}:LiSAF lasers using a rate equation system extended to multi-wavelength. Broadband emission and absorption spectra of the Cr^{3+}: LiSAF laser medium and the Cr^{4+}:YSO saturable absorber have been respected in the investigation. As a result, the obtained results showed clearly the temporal and spectral processes, and therefore, provided better understanding of CW diode-end-pumped passively Cr^{4+}:YSO Q-switched solid-state Cr^{3+}:LiSAF lasers in broadband and tunable laser operations. Laser characteristics of tunable passively Q-switched laser operation have been demonstrated to be as functions of wavelength. Spectro-temporal evolution of a single pulse from the passively Q-switched Cr^{3+}:LiSAF lasers has been reported.

Table 1. Material properties of Cr:YSO [4].

Chemical formula	Cr^{4+}: Y_2SiO_5
Crystal system	Monoclinic, biaxial
Lattice constants	a = 10.41 Å, b = 6.72 Å, c = 12.49 Å, β = 102^{o}39'
Cr atoms / mole %	$\sim 9.7 \times 10^{19}$ /cm^3
Refractive index	1,8
Main absorption peaks	390 nm, 595 nm, 695 nm, and 750 nm
Absorption spectrum	300 nm to 950 nm
Emission spectrum	1000 nm to 1500 nm (peaked at $\sim$ 1250 nm)
Fluorescence lifetime at 25 ^{o}C	$\sim 0.7 \mu$s
Density	4.6 g/cm^3

Table 2. Material properties of Cr:LiSAF [2].

Chemical formula	Cr^{3+}: $LiSrAlF_6$
Crystal system	Rhombohedral, uniaxial
Main absorption peaks	440 nm and 650 nm
Emission spectrum	700 nm to 1100 nm (peaked at $\sim$ 830 nm)
Peak laser wavelength	$\sim$ 850nm
Peak emission cross-section	$\sim 4.8 \times 10^{-20}$cm^2
Fluorescence lifetime at 25 ^{o}C	$\sim 67\mu$s
Refractive index	$\sim$ 1.41

II. LASER MODEL AND RATE EQUATION SYSTEM EXTENDED TO MULTI-WAVELENGTH

We consider a diode end-pumped solid-state Cr:LiSAF laser passively Q-switched with a Cr:YSO saturable absorber, as shown in Fig. 1.

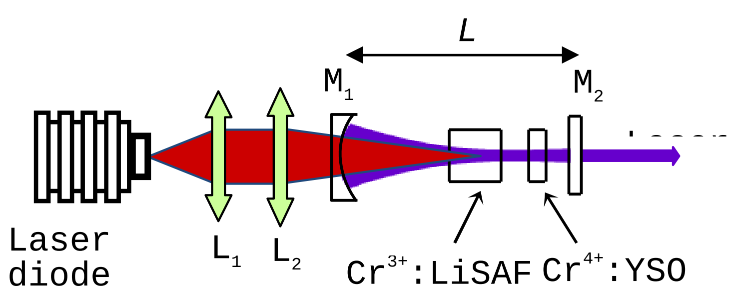

Fig. 1. Schematic diagram of a diode end -pumed solid-state Cr:LiSAF laser passively Q-switched with a Cr:YSO saturable absorber.

For computation, a system i+ 2 of rate equations extended to multi-wavelengths for i wavelength is used as follows [3, 20–22]:

$$\frac{dN_g}{dt} = R_P + \left(\sum_{i=1}^{k} \sigma_{ai} I_i\right) N_0 - \left[\frac{1}{\tau_g} + \sum_{i=1}^{k} \sigma_{ei} I_i\right] N_g \tag{1}$$

$$\frac{dI_i}{dt} = \left[2l_g(\sigma_{ei}N_g - \sigma_{ai}N_0) - 2\sigma_{a_{1i}} l_a N_a - 2\sigma_{a_{2i}} l_a (N_{a0} - N_a) - \delta\right] \frac{I_i}{T_r} + \varepsilon_i N_g \tag{2}$$

$$\frac{dN_a}{dt} = (N_{a0} - N_a)\frac{1}{\tau_a} - N_a \left(\sum_{i=1}^{n} \sigma_{a_{1i}} I_i\right) \tag{3}$$

$$N = N_g + N_0 \tag{4}$$

$$R_P = \frac{P_p\left[1 - \exp(-\alpha l_g)\right]}{h\nu_p A l_g} = \frac{P_p\left[1 - \exp(-\alpha l_g)\right]\lambda_p}{hc\pi r_p^2 l_g};\ \alpha = \sigma_p N \tag{5}$$

where,

N_0	the population density of the ground state of the active medium	cm^{-3}
N_g	the population density of the excited state of the active medium	cm^{-3}
N	the total doping density of the active medium	cm^{-3}
I_i	the laser intensity at wavelength λ_i	$cm^{-2}\mu s^{-1}$
λ_i	laser wavelength	cm
R_p	the volumetric pumping rate	$cm^{-3}\mu s^{-1}$
P_p	the pumping power at λ_p(pumping wavelength)	W
λ_p	the pumping wavelength	cm
r_p	the pumping spot radius	cm
τ_g	the fluorescence lifetime of the active medium	μs
τ_a	the fluorescence lifetime of the saturable absorber	μs
T_r	the round-trip cavity time, $T_r = 2L'c^{-1}$ with $L' = L + l_g(n_g - 1) + l_a(n_a - 1)$	μs
l_g	the length of active medium	cm
l_a	the length of the saturable absorber	cm
L	the cavity length	cm
n_g	refractive index of the active medium	
n_a	refractive index of the saturable absorber	
δ	the total round-trip losses, $\delta = -\ln(R_1R_2) + \delta_1$	
	(δ_1 is different losses due to absorption, diffraction and scattering intra-cavity)	
R_1	the reflectivities of end mirror at the laser wavelength ($R_1 \approx 1$)	
R_2	the reflectivities of output mirror at the laser wavelength	
ε_i	the constant that simulates the spontaneous emission at λ_i,	cm.μs^{-2}
σ_{ai}	the absorption cross section of the active medium at λ_i	cm^2
σ_{ei}	the stimulated emission cross section of the active medium at λ_i	cm^2
N_{a0}	the total population density of saturable absorber, $N_{a0} = -\ln(T_0)/\sum_i \sigma_{a1i} l_a$	cm^{-3}
T_0	the intinial transmission of the saturable absorber	
N_a	the ground-state population density of the saturable absorber	cm^{-3}
σ_{a1i}	the ground state absorption cross-sections of saturable absorber at λ_i	cm^2
σ_{a2i}	the excited state absorption cross-sections of saturable absorber at λ_i	cm^2

α	the absorption coefficient at λ_p	cm^{-1}
h	Planck's constant	J.μs
c	the velocity of light in vacuum	cm/μs

The output performance of the laser system such as the output energy E_{out}, the peak power P_{peak} and the approximate FWHM pulse duration t_p of the passively Q-switched laser pulse can be written as:

$$E_{out} = \frac{A}{2}\left(\sum_{i=1}^{k}\frac{hc}{\lambda_i\sigma_{ei}}\right)\ln\left(\frac{1}{R_2}\right)\ln\left(\frac{N_i}{N_f}\right) \tag{6}$$

$$P_{peak} = \frac{\pi r_l^2 L'}{cT_r}\left(\sum_{i=1}^{k}\frac{hc}{\lambda_i}\right)\ln\left(\frac{1}{R_2}\right)\left[N_i - N_t - N_t\ln\left(\frac{N_i}{N_t}\right)\right] \tag{7}$$

$$t_p = \frac{E_{out}}{P_{peak}} \tag{8}$$

where, L' is the optical length of the cavity; A is the cross-sectional area of the laser beam, $A = \pi r_l^2$; N_i is the initial population inversion density at the start of Q-switching and N_f is the final inversion population density at the end of Q-switching in the generating medium.

Table 3. Parameters used for computation

Parameters	***Value***
Pump (CW diode)	λ_p= 670 nm (pumping wavelength)
	r_p =80 μm (pumping mode radius)
	P_p = 1 ÷ 5 W
Active medium (Cr^{3+}: $LiSrAlF_6$) [4, 14]	n_a = 1.41; l_g = 0.4 cm
	N = 25.125 × 10^{19} ions.cm^{-3} (Cr^{3+}: at. 3%, α = 18 cm^{-1})
	τ_g = 67 μs; $\varepsilon_i = 10^{-12}$ cm.s^{-2}
	σ_{ei}, σ_{ai} and $\sigma_p = 4.3 \times 10^{-20}$ cm^2 [4, 14]
Absorber (Cr^{4+}: Y_2SiO_5)	l_a = 0.1 cm, n_a = 1.8, τ_a = 0.7 μs
	σ_{a1i} and σ_{a2i} with $\sigma_{a2i}/\sigma_{a1i}$ = 0.33 [4]
	T_0 = 80 ÷ 98 %
Cavity	L = 5 ÷ 50 cm
	R_1 = 1; R_2 = 0.8 ÷ 0.99
	r_l =80 μm (laser mode radius)
	δ_1 =1 % (different losses intracavity)
Spectral selector (Birefringent filter)	d =0.3 mm
	A =32^o – 54^o (tuning angle)
Velocity of light	c = 3.10^4 cm/μs
Planck's constant	h =6.625 × 10^{-28} J.μs

We numerically solve the rate equations extended to multi-wavelengths for i wavelength to investigate the performances of a broadband passively Cr:YSO Q-switched Cr:LiSAF laser and a tunable passively Cr:YSO Q-switched Cr:LiSAF laser. In the tunable Q-Switched laser operation, a birefringent filter (BF) plate was used intracavity as a spectral selector. We used 53 coupled equations, one equation for the population density of the excited state of the gain medium, one equation for the population density of the saturable absorber and 51 the monochromatic intensities at wavelength between 830 – 880 nm chosen at a constant spectral interval of 1 nm. The parameters used in the computations are collected in Table 3.

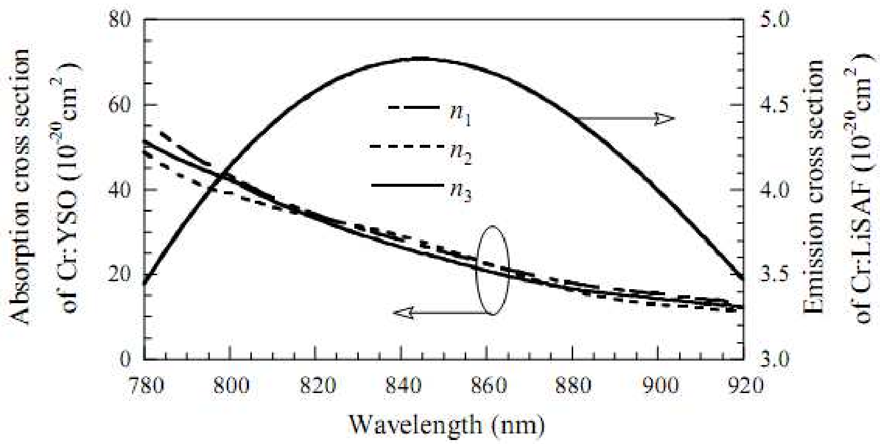

Fig. 2. Polarized absorption spectra of the Cr:YSO saturable absorber and emission cross section of the Cr:LiSAF laser as a function of wavelength ranging from 780 nm to 920 nm along each of the three principal axes [4].

The spectral parameters of broadband emission spectra of Cr:LiSAF laser crystal and the broadband absorption spectra of Cr:YSO saturable absorber were provided from Ref. [4]. Fig. 2 presents the polarized absorption spectra of the Cr:YSO saturable absorber and emission cross section of the Cr:LiSAF laser as a function of wavelength ranging from 780 nm to 920 nm along each of the three principal axes [4, 14]. For following studies, it is assumed that the laser polarization is along the n_3 axis of the Cr:YSO saturable absorber.

III. RESULTS AND DISCUSSION

Broadband Q-switched laser operation

Fig. 3 presents N_g, *Loss* and *I*intensity of the passively Cr:YSO Q-switched Cr:LiSAF laser as a function of time when R_2 = 95 %; T_0 = 90 %; L = 5 cm; P_p = 2.5 W. The results indicate that, when the intra-cavity light intensity is weak, the loss of the Cr:YSO Q-switched Cr:LiSAF laser is large and has an initial value of about 1.78×10^{18} ions.cm^{-3}. The laser should be pumped so that the gain will be greater than the loss i.e., $N_g > Loss$. When this condition is satisfied the intra-cavity light intensity will start to build up from the noise by depleting the laser population inversion density, and the Cr:YSO saturable absorber will start to saturated. When the intra-cavity light intensity increases, the loss decreases accordingly as a result of the bleaching effect of the Cr:YSO saturable absorber. The intra-cavity light intensity reaches its peak when the laser population inversion density is equal to the cavity loss, i.e., when $N_g = Loss \approx 1.76 \times 10^{18}$ ions.cm^{-3}. Beyond this point the laser gain is smaller than the total loss, and the Q-switched laser pulse is exhausted and disappears rapidly while the population inversion density decreases also quickly to a minimum value of about 1.5×10^{18} ions.cm^{-3}.The increase of the cavity loss after the release of the Q-switched laser pulse is due to the relaxation of the saturable absorber population. As a result of CW laser diode pumping, the population inversion density N_g that does not decrease to zero after the release of Q-switched laser pulse, will start to increase for the generation of the next Q-switched laser pulse.

Fig. 3 shows that the first Q-switched pulse is developed at a time of 21.35 μs after the pumping starts. This time is so-called the time required for the developing the first Q-switched pulse (The higher the diode pump power, the shorter this time). However, the time interval between two adjacent Q-switched laser pulses becomes constant and it is 5.65 μs in the case. In other words, the passively Q-switched laser pulses are a regular pulse train generated at a repetition rate of about 177 kHz.

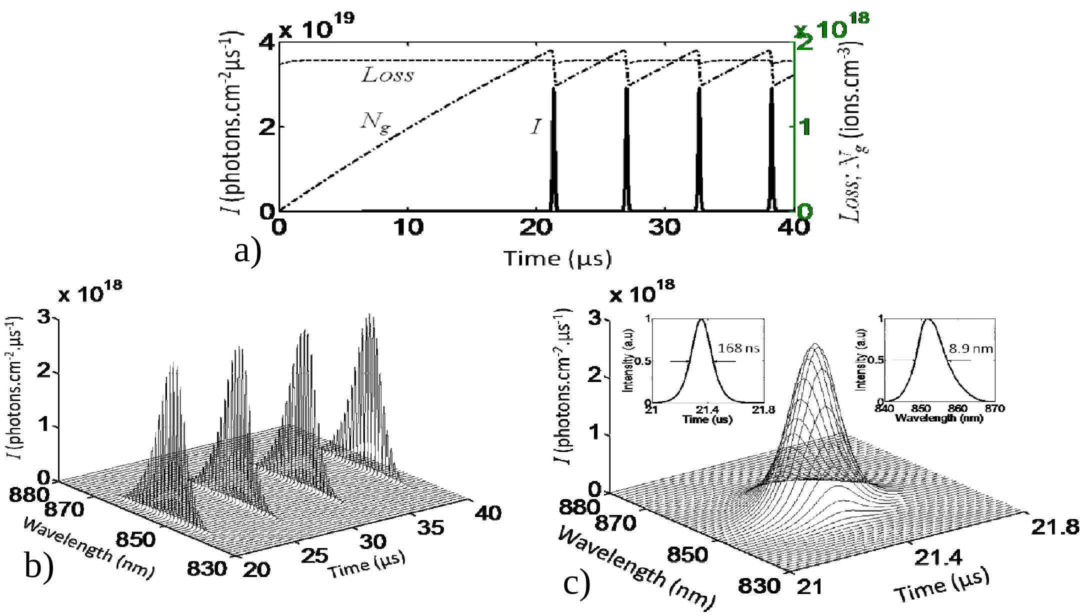

Fig. 3. a) Temporal processes of the passively Cr:YSO Q-Switched Cr:LiSAF laser pulse when R_2 = 95 %; T_0 = 90 %; $L = 5$ cm; $P_p = 2.5$ W, b) 3D presentation of temporal and spectral processes as shown in Fig. 3a, and c) temporal and spectral evolution of a single Q-Switched Cr:LiSAF laser pulse. The insets show it integrated laser spectrum with a linewidth of 8.9 nm and a pulsewidth of 168 ns.

Fig. 3b presents the 3D presentation of the processes as shown in Fig. 3a in respect to laser wavelength. The spectro-temporal evolution of a single broadband Q-switched laser pulse was presented clearly in Fig. 3c. Each of the broadband Q-switched laser pulses has a pulsewidth of 168 ns, a bandwidth of 8.9 nm and a pulse energy of about 310 μJ given by (6).

Figures 4 and 5 present the pulse width, output laser energy and repetition rate of the broadband passively Q-switched Cr:LiSAF laser pulse as a function of reflectivity of output mirror for several values of T_0 of Cr:YSO saturable absorber when P_p = 2.5 W; L = 5 cm (Fig. 4) and for several values of L when P_p = 2.5 W; T_0 = 90 % (Fig. 5). The simulation results indicate that broadband passive Q-switching performance becomes better while R_2 from 0.9 to 0.98 and T_0 (Fig. 4) and L decreased (Fig. 5). However, when L became shorter, output laser energy is also decreased.

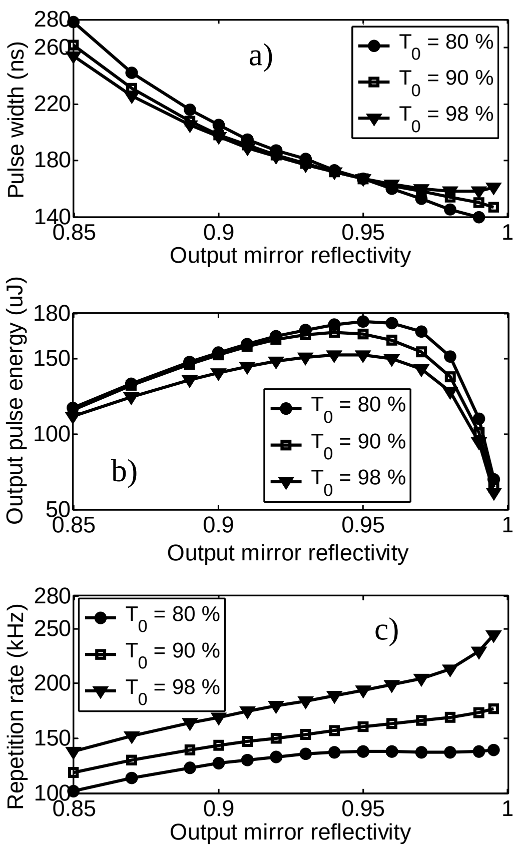

Fig. 4. a) Laser pulse width, b) Output pulse energy, and c) repetition rate of the passively Q-switched Cr:LiSAF laser pulse as a function of output mirror reflectivity with different initial transmissions of Cr:YSO saturable absorber when $P_p = 2.5\,\mathrm{W}$; $L = 5\,\mathrm{cm}$

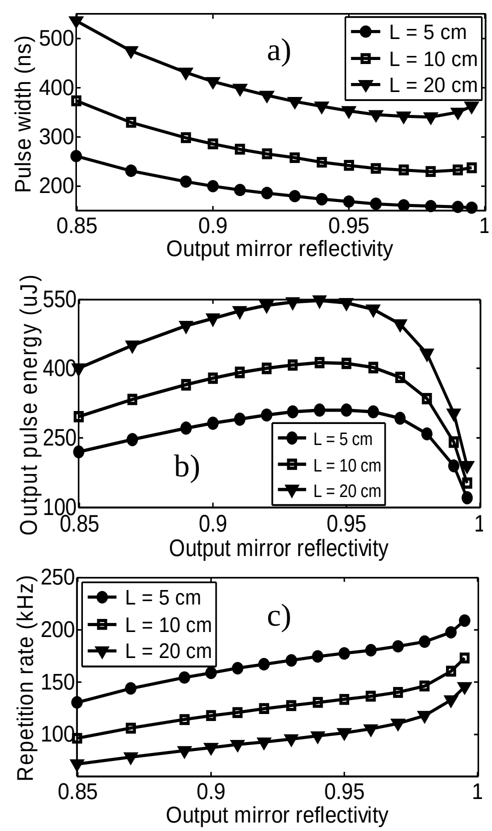

Fig. 5. a) Laser pulse width, b) Output pulse energy, and c) repetition rate of the passively Q-Switched Cr:LiSAF laser pulse as a function of output mirror reflectivity with different cavity length when $P_p = 2.5$ W; T_0 = 90 %.

Figures 6 and 7 show the pulse width, output laser energy and repetition rate of the broadband passively Q-switched Cr:LiSAF laser pulse as a function of pump diode power for several values of R_2 when T_0 = 90 %; L = 5 cm (Fig. 6) and power for several values of T_0 when L = 5 cm; R_2 = 95% (Fig. 7). It is obvious that better laser performance can be obtained with higher pumping diode power.

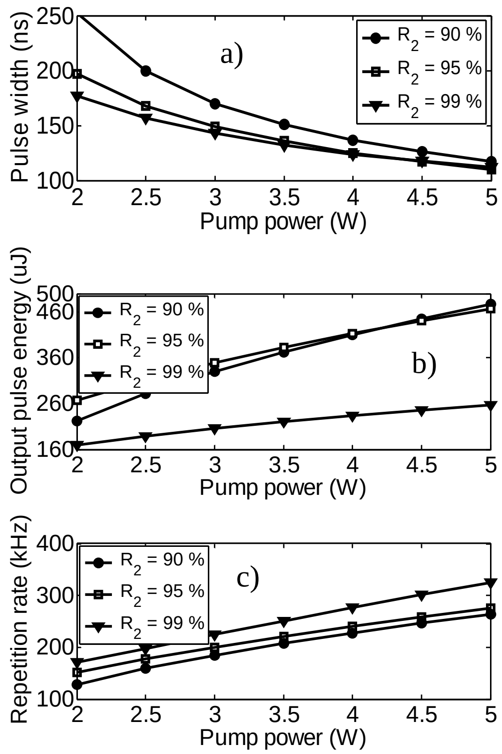

Fig. 6. a) Laser pulse width, b) Output pulse energy, and c) repetition rate of the passively Q-switched Cr:LiSAF laser pulse as a function of pump diode power with different output mirror reflectivity when T_0 = 90 %; L = 5 cm.

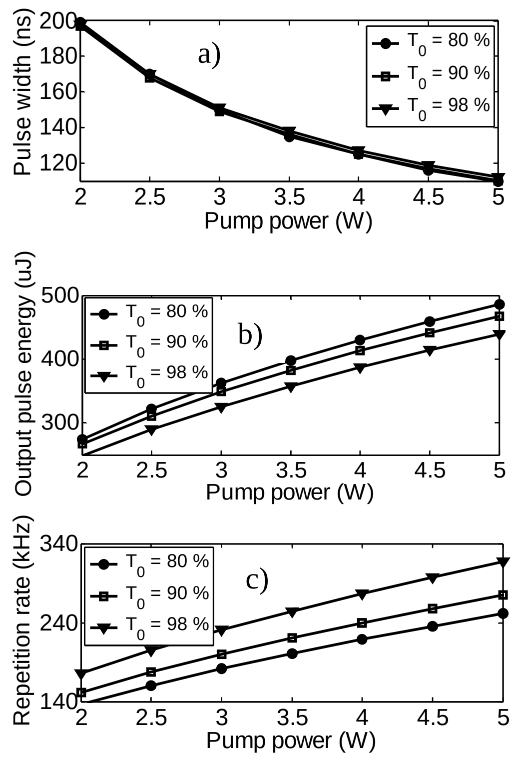

Fig. 7. a) Laser pulse width, b) Output pulse energy, and c) repetition rate of the passively Q-Switched Cr:LiSAF laser pulse as a function of pump diode power with different initial transmissions of Cr:YSO saturable absorber when L = 5 cm; R_2 = 95 %.

The numerically obtained results presented in Fig. 4 - Fig. 7 are the laser characteristics of the broadband passively Q-switched Cr:LiSAF lasers, our results are in a good agreement with those obtained experimentally and numerically by other research groups [3-5, 13,14].

Fig. 8a) presents the effects of the initial transmissions of Cr:YSO saturable absorber on peak position and bandwidth of the integrated laser spectra of the broadband passively Q-switched Cr:LiSAF laser pulse when L = 5 cm; R_2 = 95 % and P_p = 2.5 W. Fig. 8b) shows the effects of pump diode power on bandwidth of the integrated spectra of the broadband passively Q-Switched Cr:LiSAF laser pulse when L = 5 cm; R_2 = 95 % and T_0 = 90 %. While the initial transmission of Cr:YSO was increasing, the bandwidth of the integrated laser spectra became narrow, and simultaneously a short-wavelength shift of its peak position was observed, however, the bandwidth of the integrated laser spectra is not sensitive with pump diode power.

Tunable Q-switched laser operation:

A tunable passively Q-Switched laser operation was obtained with a birefringent filter plate used as an intra-cavity spectral selector. The birefringent filter plate is used for the incident beam

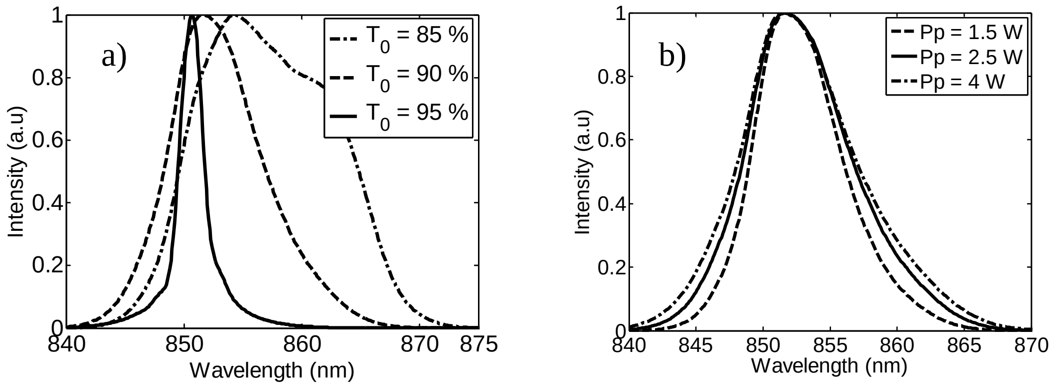

Fig. 8. Dependence of integrated laser spectra of the passively Q-switched Cr:LiSAF laser pulse on initial transmissions of Cr:YSO saturable absorber when L = 5 cm; R_2 = 95 % and P_p = 2.5 W (a) and on pump diode power when L = 5 cm; R_2 = 95 % and T_0 = 90 % (b).

at Brewster angle. The transmission function of this BF plate was given by [23]:

$$T(\lambda) = 1 - 4\cot^2\gamma\tan^2\theta\left(1 - \cot^2\gamma\tan^2\theta\right)\sin^2\frac{\delta\varphi(\lambda)}{2} \tag{9}$$

where γ is the angle between the internal wave vector and the optic axis; θ is the incident angle (Brewster angle) and $\delta\varphi(\lambda)$ is the phase retardation of the BF plate, in which [23]

$$\delta\varphi(\lambda) = \frac{2\pi d\,(n_o - n_e)\sin^2\gamma}{\lambda\sin\theta} \tag{10}$$

with $(n_o - n_e)$ is the index difference between the ordinary and extraordinary rays, d is the plate thickness, λ is the wavelength of the incident ray. The tuning angle A is defined as follows [23]:

$$\cos A = \frac{\cos\gamma - \sin\theta\sin\beta}{\cos\theta\cos\beta} \tag{11}$$

where β is the angle between the optic axis and the BF plate surface.

For comparative studies with the broadband passively Q-switched laser operation, we used the same laser parameters and the tunable passively Cr:YSO Q-switched Cr:LiSAF laser was tuned to 802 nm with a birefringent filter plate of 0.3 mm thickness at tuning angle A = 32^o. Hence, the performance of such a tunable passively Q-switched Cr:LiSAF laser is similar as that of a broadband passively Q-switched Cr:LiSAF laser with an additional dependent-wavelength loss due to the BF plate.

We numerically solve the rate equations extended to multi-wavelengths for i wavelength to investigate the performance of the tunable passively Cr:YSO Q-switched Cr:LiSAF laser system when P_p = 2.5 W; L = 5 cm; T_0 = 90 %; R_2 = 95 %; BF: d = 0.3 mm; β = 0, tuning angle A=32^o corresponding to the laser wavelength at 802 nm. The other parameters used in this computation are collected in Table 3. In the case, the total cavity losses containing the output coupler loss, saturable absorber loss and dependent-wavelength loss due to the birefringent filter is given by:

$$\delta(\lambda) = -\ln\left[R_1R_2\cdot T^2(\lambda)\right] + \delta_1 \tag{12}$$

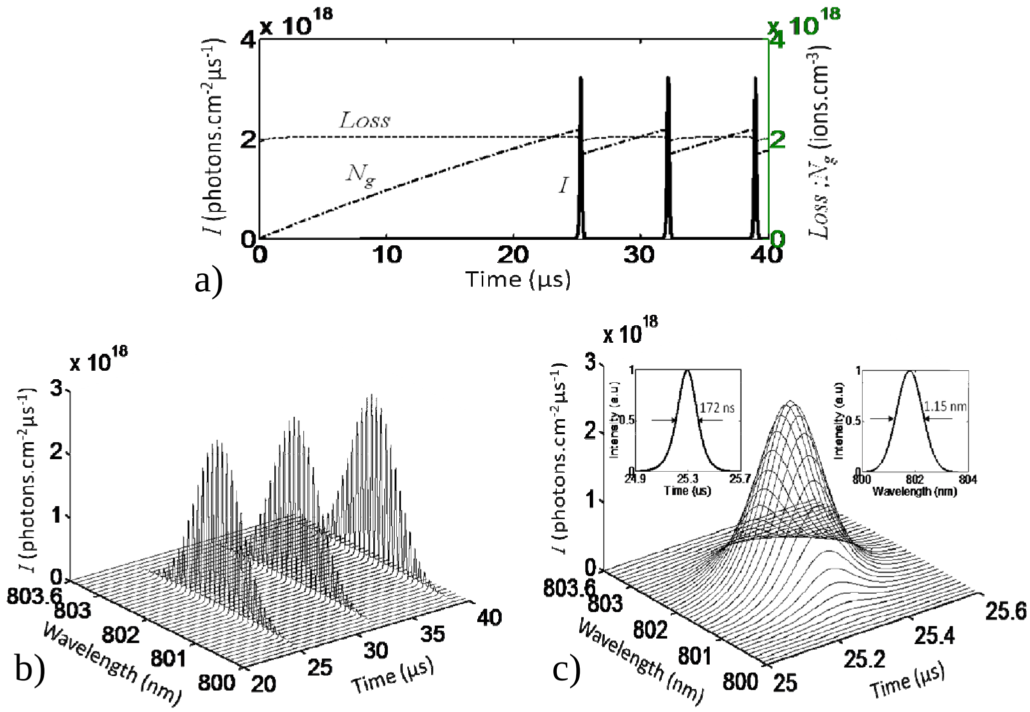

Fig. 9. a) Temporal and spectral processes of the tunable passively Q-switched Cr:LiSAF laser tuned at 802 nm when P_p = 2.5 W; L = 5 cm; T_0 = 90 %; R_2 = 95 %; BF: d = 0.3 mm; β = 0, tuning angle A = 32^o, b) 3D presentation of temporal and spectral processes as shown in Fig. 9a in respect to wavelength, and c) temporal and spectral evolution of a single tunable Q-switched laser pulse. The insets show its integrated laser spectrum with a linewidth of 1.15 nm and a pulsewidth of 178 ns.

Fig. 9a) presents the temporal processes of the tunable passively Q-Switched Cr:LiSAF laser when $P_p = 2.5$ W; $L = 5$ cm; $T_0 = 90\%$; $R_2 = 95\%$; BF: $d = 0.3$ mm; $\beta = 0$, the laser was tuned to the wavelength of 802 nm with the BF plate of tuning angle A of 32°. In this case, the time interval between two adjacent Q-switched laser pulses is constant and about 6.88 μs. The narrowband Q-switched laser pulses are a regular pulse train generated at a repetition rate of 146 kHz.

Fig. 9b) shows the 3D presentation of the temporal and spectral processes of the tunable passively Q-switched Cr:LiSAF laser, as shown in Fig. 9a. Fig. 9c shows the temporal and spectral evolution of a single tunable Q-switched laser pulse at $\sim$ 802 nm. The numerically obtained results show the bandwidth of integrated laser spectrum to be 1.15 nm, a pulsewidth of 178 ns and a pulse energy of 1.71 mJ given by (6).

Similarly, we numerically solve the rate equations extended to multi-wavelengths for i wavelength to search the spectral range for tuning wavelength of the tunable passively Cr:YSO

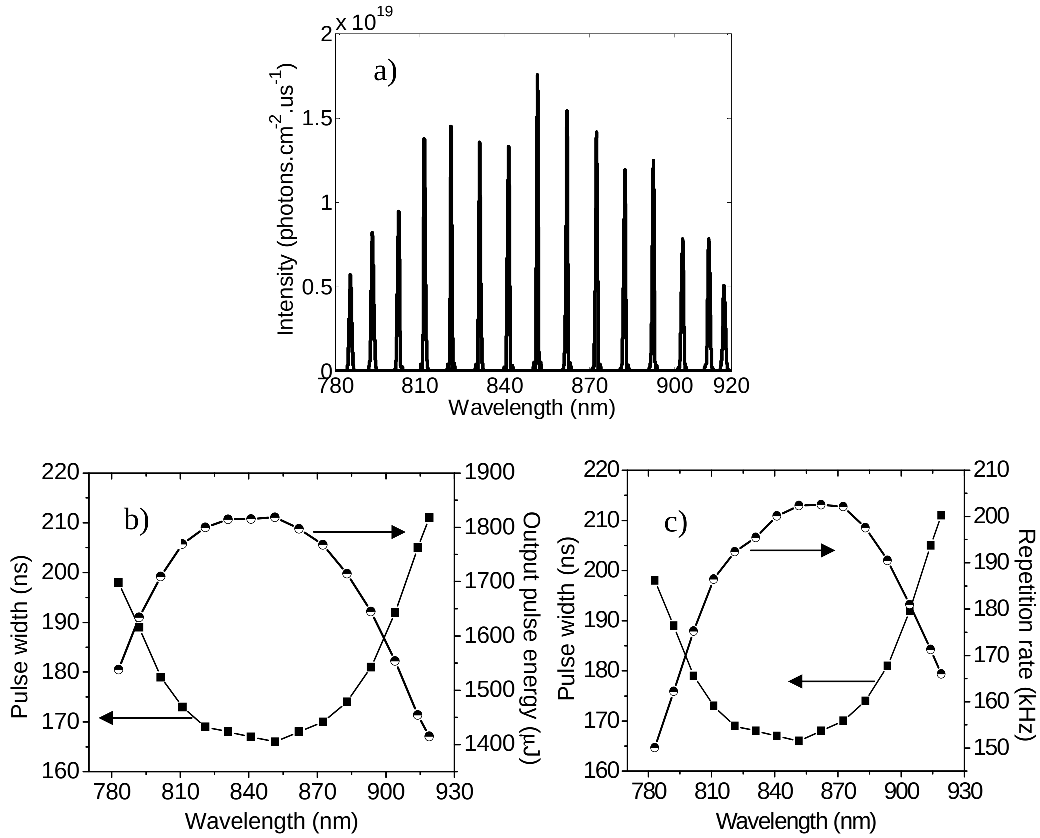

Fig. 10. a) Spectral range for tuning wavelength from 780 - 920 nm of the tunable passively Q-switched Cr:LiSAF laser when P_p = 2.5 W; L = 5 cm; T_0 = 90 %; R_2= 95 %; Birefringent Filter: d = 0.3 mm; β = 0, the tuning angle A was varied from 28° to 54°; b) Laser pulsewidth and output pulse energy and c) repetition rate of the tunable passively Q-switched laser pulse as a function of wavelength.

Q-switched Cr:LiSAF laser system when P_p = 2.5 W; L = 5 cm; T_0 = 90 %; R_2 = 95 %; BF: d = 0.3 mm; β = 0 and the tuning angle A is varied from 28^o to 54^o.

Fig. 10 presents the spectral range for tuning laser wavelength from 780 - 920 nm of the tunable passively Q-switched Cr:LiSAF laser when the birefringent filter plate was tuning from 28^o to 54^o. The spectral tuning range was obtained experimentally or numerically by other research groups [4-6,19]. The results also indicate that the laser characteristics of the tunable passively Q-switched Cr:LiSAF laser depend clearly on laser wavelength. Fig. 10b and Fig. 10c show that pulse width, output pulse energy and repetition rate of the tunable passively Q-switched Cr:LiSAF laser pulse are as functions of wavelength. It is noteworthy that the absorption of Cr:YSO saturable absorber is large considerably in the short laser wavelength region (shorter than 825 nm), our results are quite different from those obtained by a single-frequency analysis [4–6] where homogeneously broadened emission spectra of Cr:LiSAF laser crystal and broadband absorption spectra of Cr:YSO saturable absorber were neglected. These simulation results are in a good agreement with those obtained experimentally in the wavelength region (longer than 825 nm) [3–5, 13, 14]. Experiments to investigate the characteristics of such a tunable passively Cr:YSO Q-switched Cr:LiSAF laser has been carried out and presented in detail in elsewhere.

IV. CONCLUSION

Using a rate equation system extended to multi-wavelength, we have numerically investigated, for the first time, the performances and characteristics of CW diode-end-pumped, passively Cr:YSO Q-switched Cr:LiSAF lasers in broadband and tunable laser operations. Homogeneously broadened emission spectra of Cr:LiSAF laser crystal and broadband absorption spectra of Cr:YSO saturable absorber were respected in the investigation. As results, improved understanding of the passively Q-switched Cr:YSO Cr:LiSAF laser operations has been obtained. Laser characteristics of the tunable passively Q-switched laser operation were as functions of wavelength, and particular, different from those obtained in the short laser wavelength region of previous single-frequency investigations. The spectro-temporal evolutions of a single pulse from the broadband and tunable passively Q-switched Cr:LiSAF lasers have been reported.

ACKNOWLEDGMENT

The authors would like to thank for the financial support from Vietnam NAFOSTED (Physics, Project No. 103.06.89.09).

REFERENCES

[1] W. Demtroder, *Laser Spectroscopy. Basic Concepts and Instrumentation*. Third edition. Springer - Verlag, Berlin Heidelberg, 2003.
[2] W. Koechner, *Solid-State Laser Engineering*, 5^{th} edition, Springer-Verlag, Berlin Heidelberg, 1999.
[3] Y.-K. Kuo, M.-F. Huang, and M. Birnbaum, *IEEE J. Quantum Electron*. **31** (1995) 657−663.
[4] H. F Chen, S.W. Hsieh, Y.K. Kuo. *High Power Lasers and Applications III*, *Proceedings of SPIE* **5627** (2005) 488-498.
[5] H. F Chen, S. W. Hsieh, Y. K. Kuo. *High Power Lasers and Applications II*, Proceedings of SPIE **4914** (2002) 498- 509.
[6] N. V. Hao, N. D. Hoang, Ngo K. Quang et al., *Computational Methods in Science and Technology*, Special issue (2), (2010) 27-31.
[7] N. T. Nghia, D. Q. Khanh, T. D. Huy, L. T. T. Nga, N. D. Hung, ASEAN *Journal on Science & Technology for Development* **24**(1-2) (2007) 139-146.
[8] N. T. Nghia, N. V. Hao, V. A. Orlovich, N. D. Hung, *Quantum Electronics*, **41**(9) (2011) 790 - 793.
[9] N. T. Nghia, D. Q. Khanh, N. D. Hung, and P. Brechignac, *Communications in Physics*, **19** (Special Issue) (2009) 145-155.
[10] W. Chen, K. Spariosu, R. Stultz, Y.-K. Kuo, M. Birnbaum, and A. V. Shestakov, *Opt. Commun.* **104** (1993) 71-74.
[11] Y.-K. Kuo and M. Birnbaum, *Appl. Phys. Lett.* **67** (1995) 173 – 175.
[12] E. Munin, A. B. Villaverde, X. X. Zhang, and M. Bass, *Appl. Phys. Lett.* **63** (1993) 1739-1741.
[13] E. Beyatli, A. Sennaroglu, U. Demirbas, *J. Opt. Soc. Am. B* **30**(4) (2013) 914-921.
[14] S. A. Payne, L. L. Chase *et al.*, *J. Appl. Phys.* **66** (1989) 1051-1056; S. A. Payne, L. L. Chase, G.D. Wilke, *J. of Luminescence* 44 (1989) 167; S. A. Payne, W.F. Krupke, L. L. Chase *et al. IEEE J. of Quantum Electron*. *QE-* **28** (1992) 1188.
[15] M. J. P. Dymott and A. I. Ferguson, *Opt. Lett.* **19** (1994) 1988 – 1990.
[16] P. A. Beaud, M. Richadson, and E. J. Miesak, *IEEE J. Quantum Electron*. **31** (1995) 317 – 325.
[17] S. Makio, M. Sato, T . Sasaki. *Jpn. J. Appl. Phys*. **40** (2001) 2278-2281.

[18] C. S. Chen, Y. S. Zang, J. W. Yu J. Fang, S. H. Liu. *Chin. Phys. Lett*. **26**(9) (2009) 094206.
[19] M. Stalder, B. H. T. Chai, and M. Bass, *Appl. Phys. Lett.* **58** (1991) 216−218.
[20] W. G. Wagner and B. A. Lengyel, *Journal of Applied Physics* **34** (1963) 2040-2046.
[21] A. Szabo and R. A. Stein, *Journal of Applied Physics* **36** (1965) 1562-1566.
[22] N. D. Hung, Y. Segawa, P. Long, et.al, *Appl. Phys. B* **65** (1997) 19-26.
[23] Xinglong Wang and Jianquan Yao, *Appl. Opt*. **31**(22) (1992) 4505 – 4508.